Aero-Self-Assembly of Ultrafine Gold Incorporated Silica Nanobunches for NIR-Induced Chemo-Thermal Therapy

Jeong Hoon Byeon and Young-Woo Kim**

The application of nanomaterials in biomedicine is an important part of the developing nanotechnology field. In particular, hybrid nanoparticles or nanocomposites containing two or more different nanoscale functionalities are attractive candidates for advanced nanomaterials.[1] With a controlled structure and interface interactions, these nanoparticles can exhibit novel physical and chemical properties that will be essential for future technological applications.[2] The structure offers two functional surfaces for the attachment of different kinds of molecules, making such species especially attractive as multifunctional probes for diagnostic and therapeutic applications.[3]

Gold (Au) decorated silica (SiO_2), Au-SiO_2, hybrid nanoparticles represent one such multifunctional system. Combinations of SiO_2 with Au nanoparticles offer possibilities for the development of interesting advanced composite materials as a result of bringing together their plasmonic properties and biocompatibility.[4] Furthermore, when the nanoparticles are irradiated, the surface plasmon resonance (SPR) absorption of Au nanoparticles is followed by rapid conversion of light into heat, due to the collective oscillations of their delocalized conduction electrons.[5] When excited by resonance, energy not reradiated through light scattering is dissipated through Landau damping, resulting in a dramatic rise in temperature in the nanoscale vicinity of the particle surface.[6] In biomedicine, this unique property can be exploited for applications such as photothermal ablation and thermosensitive drug delivery.[7] Clinically, the optimal wavelengths for the laser radiation of Au nanoparticles are within the biological near infrared (NIR) region.

Many efforts have been made to synthesize bifunctional nanomaterials combining SiO_2 and Au in liquid-phase.[8] To synthesize these nanoparticles, a judicious selection of reaction conditions is needed to promote heterogeneous nucleation of a target solid onto preformed nanocrystal seeds while avoiding conditions that result in isolated single-component particles. When these methods are applied to deposit Au on SiO_2, the average diameter of Au particles becomes very large (20 nm).[9] Moreover, the nanoparticles and their syntheses are becoming increasingly complex, time-consuming, and complicated, and have the potential to form multiple products in the reaction solution.[10] Therefore, more effort is required to realize efficient self-assembly of Au incorporated SiO_2 particles at the nanoscale in order to complement the already mature techniques in wet chemistry.[11]

The present work introduces a continuous gas-phase-based self-assembly to fabricate Au-SiO_2 hybrid nanoparticles incorporating with ibuprofen (IBU) and poly-l-lysine (PLL) for efficient inhibition in proliferation of HeLa cells under NIR light irradiation (see **Scheme 1**). The gas-phase-based fabrication may give birth to a promising family of innovative nanomaterials with many desirable applications, both realized and potential, in biomedical domains, such as functional coatings, biomaterials, multifunctional therapeutic carriers, and controlled release.[12] Freshly gas-phase produced Au nanoparticles were created and the particle-laden flow passed over the atomizer orifice where they mixed with the atomized SiO_2/IBU-PLL to form hybrid droplets. The droplets then passed through a denuder to drive solvent from the droplets, resulting in Au-SiO_2/IBU-PLL functional nanoparticles. These nanoparticles were then employed as both nanoscale drug carriers and transducers to facilitate the thermal IBU release to HeLa cells by SPR heating of the nanoparticles.

To prepare fresh Au nanoparticles in the gas-phase, a spark discharge under nitrogen environment was employed. The gas temperature inside the spark channel was increased beyond a critical value, which was sufficient to sublimate parts of the Au electrodes.[13] The duration of each spark was very short (~1 ms) and the vapors cooled rapidly downstream of the spark. This formed a supersaturation resulting in particle formation through nucleation-condensation. The total number concentration (TNC), geometric mean diameter (GMD), and geometric standard deviation (GSD) of the Au particles, which were measured using a scanning mobility particle sizer (3936, TSI, US), were 5.24×10^6 particles cm^{-3}, 33.2 nm, 1.49, respectively, as shown in **Figure 1**. Au-SiO_2 nanoparticles were formed by incorporating Au with SiO_2 during the collison atomization of the SiO_2 solution. We verified the incorporation of the Au nanoparticles and the SiO_2 domains by measuring the size distributions of the SiO_2 and

Dr. J. H. Byeon
Department of Chemistry
Purdue University
Indiana 47907, United States
E-mail: jbyeon@purdue.edu
Dr. Y.-W. Kim
Department of Automotive Engineering
Hoseo University
Asan 336-795, South Korea
E-mail: ywkim@hoseo.edu

DOI: 10.1002/smll.201303752

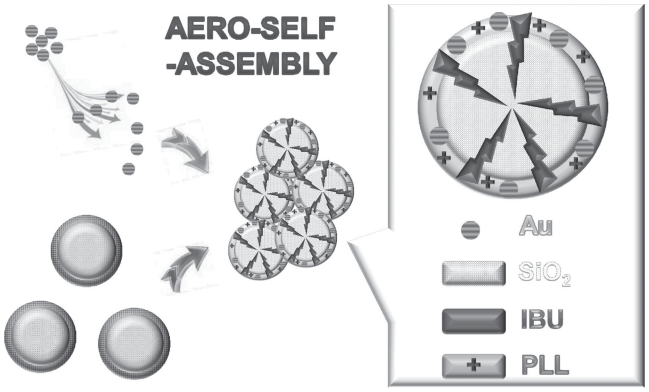

Scheme 1. Continuous aero-self-assembly to fabricate Au-SiO_2/IBU-PLL functional nanobunches

Au-SiO_2 particles in the gas-phase. Table SI summarizes the size distribution measurements of the SiO_2 and Au-SiO_2 particles. The TNC, GMD, and GSD of the Au-SiO_2 particles were 2.31×10^6 particles cm^{-3}, 81.2 nm and 1.71, respectively. The analogous data for the individual SiO_2 particles were 2.74×10^6 cm^{-3}, 78.1 nm, and 1.77, respectively. The Au-SiO_2 case shows a new size distribution compared to individual Au and SiO_2 cases, and there was no bimodal distribution characteristic, implying that the Au and SiO_2 particles were nearly quantitatively incorporated and restructured to form Au-SiO_2 nanoparticles. Even though the size distributions changed after further incorporation of IBU and IBU-PLL with Au-SiO_2 platforms, there were only apparent increases in concentration, not in size, which implies that the additional components were quantitatively distributed within or on the Au-SiO_2 platforms.

Low and high magnification transmission electron microscope (TEM, JEM-3010, JEOL, Japan) images show the morphology of the Au, SiO_2, and Au-SiO_2 particles. Specimens were prepared for examination in the TEM by direct electrostatic gas-phase sampling at a sampling flow of 1.0 L min^{-1} and an operating voltage of 5 kV using a Nano Particle Collector (NPC-10, HCT, Korea). The TEM images (**Figure 2**)

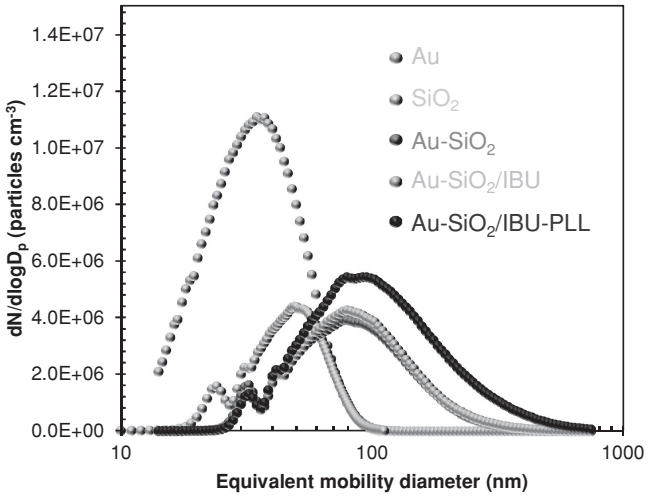

Figure 1. Size distributions of spark-produced Au, collison atomized SiO_2, and their hybridized structure (Au-SiO_2) with and without IBU-PLL from the aero-self-assembly.

reveal that the Au nanoparticles were agglomerates of several primary particles (each ~4 nm in diameter), and the morphology of the SiO_2 domains also presents agglomerates of spherical primary particles (each ~30 nm in diameter) with a size of about 80 nm in lateral dimension. When the Au agglomerates passed over the orifice of the atomizer, it was clear that dark nanodots (since Au has a higher electron density and allows the transmission of fewer electrons compared to SiO_2) were deposited onto the surface of SiO_2 particles, which confirms that the Au-SiO_2 hybrid nanoparticles had been successfully assembled. As shown in the inset of the Au-SiO_2 image, a lattice fringe size of about 0.242 nm of the Au was observed, which could be indexed as the (111) plane of the face centered cubic structure, while the mesoporous-amorphous SiO_2 structure can be seen (also refer to the insets of Figure 2).[14] The Au agglomerates were redistributed on the SiO_2 domains due to deagglomeration (by setting the force acting on an agglomerate of size D_{pa} due to the sudden pressure change across an orifice in the atomizer), and the size is given by[15]

$$D_{pr} = \alpha\sqrt{\frac{D_{pa}H}{6\pi\Delta P\Theta^2}} \quad (1)$$

where D_{pr} is the size of a restructured agglomerate, α is the proportionality constant, H is the Hamaker constant, ΔP is the pressure difference between the front and the rear of the orifice, and Θ is the parameter controlling the maximum cohesive strength between the constituting particles in an agglomerate. The Au agglomerates pass through the orifice, and the rapid changes in pressure, density, and velocity across the orifice produce an impulse capable of shattering the agglomerates. The primary Au particles are nearly quantitatively incorporated onto SiO_2, to form the Au-SiO_2 hybrid nanoparticles. This is due to heterogeneous coagulation of Au and SiO_2 before the homogeneous coagulation of Au at the position around the orifice in a collison atomizer (Scheme S2). Equation (2) describes the decrease in the number concentration of primary Au particles as a function of collisions within the Au as well as collisions with SiO_2, where the concentration is consistent:

$$\frac{dC_{Au}}{dt} \propto \left(K_{Au}C_{Au}^2 + K_{SiO_2}C_{Au}C_{SiO_2}\right) \quad (2)$$

where, C_{Au} and C_{SiO2} are the respective number concentrations of primary Au and SiO_2 particles, K_{Au} $(=\frac{4kT}{3\mu})$ and K_{SiO2} $(=\frac{2kTd_{Au}}{3\mu d_{SiO_2}})$ are the respective collision frequency functions for homogeneous and heterogeneous collisions (where k is the Boltzmann factor, T is the temperature, and μ the gas viscosity). Correspondingly, in TEM micrographs (Figure 2), Au-SiO_2 nanoparticles show deagglomerated Au and the attached Au particles being smaller and more narrowly dispersed than were the individual Au particles. Furthermore, the sizes of Au-SiO_2 nanoparticles increased with increasing coagulation time t from 0.099 to 0.909 min as also shown in Figure 2 due to the prolonged heterogeneous coagulation (Equation (2). This implies that the size and morphology of the Au-SiO_2 nanoparticles can be tuned by

NANO MICRO small

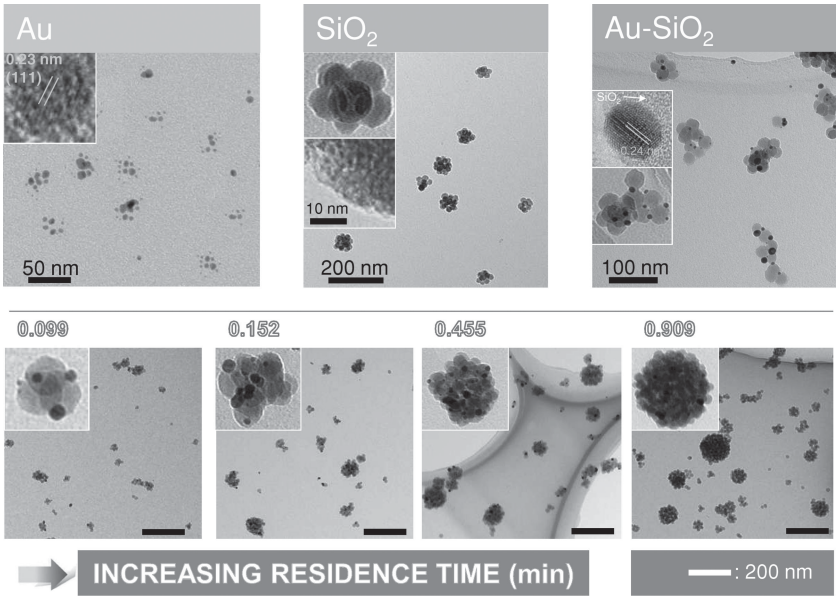

Figure 2. TEM images of spark produced Au, collison atomized SiO_2, and their hybridized structure (Au-SiO_2) from the aero-self-assembly. Different hybrid structures with increasing coagulation time between Au and SiO_2 particles are also shown.

simply controlling the coagulation time in the gas-phase. Furthermore, the sizes of Au-SiO_2/IBU-PLL nanoparticles *via* dynamic light scattering measurements were measured by zetasizer (Nano Z, Malvern, UK), with different storage days (Table SII). The results show that there are no significant differences in size between the storage days. This implies that the aero-self-assembled nanoparticles have stability that may be suitable in a long-term storage.

In Figure S1a, the spectra exhibit a plasmonic absorption at 580 nm for Au nanoparticles while the peak of Au-SiO_2 hybrid nanoparticles shifted to longer wavelength compared to the pure Au nanoparticles, which is in accordance with the Mie theory that a change of the dielectric function of the environment around the Au nanocrystals [an interaction between plasmonic responses from an Au and a SiO_2 leading to hybridization of plasmonic resonance into antisymmetric mode (higher energy) and symmetric mode (lower energy) that shows up in the visible and NIR region] can clearly induce such a shift,[16] and therefore, the synthesized Au-SiO_2 nanoparticles have NIR absorbance. Another broad band around at 400 nm for the Au-SiO_2 particles is assigned to SiO_2 particles.[17] The inset of Figure S1a shows the nitrogen adsorption isotherm of Au-SiO_2 nanoparticles. The overall shape of the Au-SiO_2 nanoparticles indicates their meso- (refer to the inset of the TEM image of Figure S1a) and macro-porous characteristics. The uptakes at >0.85 and <0.85 of P P_0^{-1} may originate from the void spaces between agglomerated Au-SiO_2 nanoparticles and the core areas of the nanoparticles, respectively. The crystallinity of the Au-SiO_2 nanoparticles was characterized by X-ray diffraction (XRD, RINT-2100, Rigaku, Japan). Figure S1b shows the XRD pattern of the Au-SiO_2 particles. There is a diffraction peak at 38.3° present in the Au-SiO_2 curve, which corresponds to the (111) plane of the Au crystal with a cubic phase (JCPDS card No. 04-0784), which indicates that the crystalline Au particles were obtained and (111) plane was preferred orientation for Au particles. Furthermore, a specific peak was observed around 23° assigned to mesoporous SiO_2,[18] indicating the nature of hybrid structures of the ultrafine Au and mesoporous SiO_2. It also can be noted that a weak intensity of SiO_2 is indicative of the long range order in SiO_2. In the inset of Figure S1b, the binding energies (BEs) at 83.3 and 86.7 eV are attributed to Au $4f_{7/2}$ and Au $4f_{5/2}$ of metallic Au. Interestingly, it is noted that the BE of Au $4f_{7/2}$ shows a negative shift compared to the 84.0 eV of bulk Au. Such a negative shift has been ascribed to a strong incorporation of Au and SiO_2.

The characteristic IBU absorption peaks of –COOH at 1720 cm^{-1} and benzene ring at 1430–1600 cm^{-1} of Au-SiO_2/IBU from Fourier transform infrared (FTIR, IFS 66/S, Bruker Optics, Germany) measurements are shown in **Figure 3**a. The weak intensity of the characteristic individual IBU bands could confirm that the IBU has been loaded in the pore of a porous Au-SiO_2 system. The characteristic bands of IBU such as the carboxyl group at 1720 cm^{-1}, the benzene ring peaks at 1430-1600 cm^{-1}, the quaternary carbon atom peaks at 1463 and 1509 cm^{-1}, and the alkyl group peaks at 2864 and 2967 cm^{-1} of the loaded IBU[19] are clearly shown in Figure S2. It can also be seen that the vibration of amide I appeared at ~1640 cm^{-1}, amide II was observed at ~1530 cm^{-1}, and that of free amino groups (NH stretching vibrations) was noticed at ~3300 cm^{-1} (inset of Figure 3b),[20] which confirms the further conjunction with PLL on both Au-SiO_2 and Au-SiO_2/IBU samples. The characteristic bands of individual PLL and mixture IBU-PLL are also shown in Figure 2S. The band at around 780 and 680 cm^{-1} of all the samples are assigned to Si-O-Si and Si-O stretching vibrations, respectively,[21] as shown in Figure 3b. In addition, even though Au particles were highly ordered on SiO_2 particles, the Au particles had no influence on the FTIR activities of the organic groups surrounding them. The inset of Figure 3a shows a TEM image of the Au-SiO_2/IBU-PLL nanoparticles, which shows brighter colored edges compared to the Au-SiO_2 nanoparticles owing to further incorporation of IBU-PLL in an Au-SiO_2 platform. We also measured the zeta potential of the Au-SiO_2/IBU-PLL dispersion in pH 7.3 is 22.1 ± 4.3 mV; this positive charge originated from amine groups of PLL indicates that the nanoparticles are electrophysiologically capable of binding to negatively charged proteins.

Figure 4a shows the behavior of Au-SiO_2/IBU-PLL nanoparticles. A polytetrafluoroethylene membrane-capped reservoir with the nanoparticles was placed in a water flow chamber and irradiated from the top surface with an 808 nm IR diode laser. The NIR triggers an enhanced release of the IBU, whose pattern is roughly coincident with the evolution of the temperature. Absorbed NIR promotes molecular oscillation leading to efficient heating of the surrounding

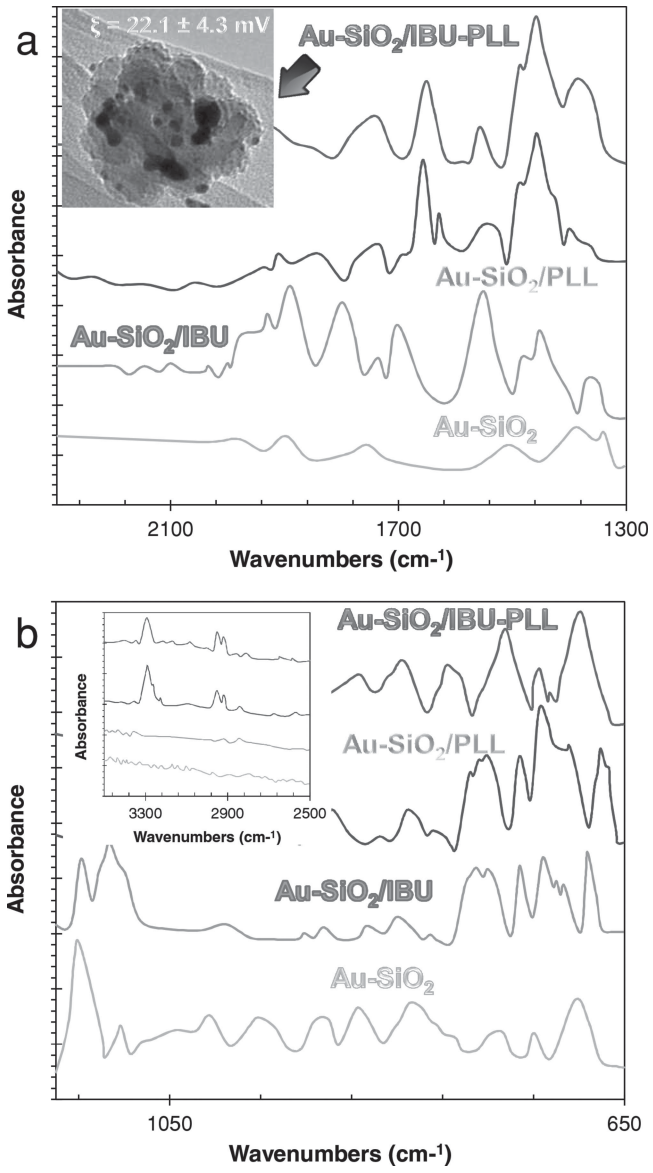

Figure 3. FTIR spectra with different frequency ranges of (a) 1300–2300 cm^{-1} and (b) 650–1150 cm^{-1} of Au-SiO_2/IBU, Au-SiO_2/PLL, and Au-SiO_2/IBU-PLL nanoparticles including pure Au-SiO_2 nanoparticles. A TEM image of Au-SiO_2/IBU-PLL nanoparticles is also shown as the inset of (a). Another FTIR spectra with different frequency range of 2500–3500 cm^{-1} are also shown as the inset of (b).

environment, which could be used as thermal transducers for enhancing IBU release. We observed a localized heating of the sample in the region exposed to laser radiation by an infrared thermometer (42545, Extech, US). The inset of Figure 4a shows the change in temperature (ΔT) of the solution containing the Au-SiO_2 nanoparticles (5–100 μg mL^{-1}); ΔT takes into account any temperature change in the control sample. The ΔT increased significantly by increasing nanoparticle concentration, hence, the maximum value of ΔT (16.4 °C) was observed at the highest concentration (100 μg mL^{-1}). The results indicated that the Au-SiO_2 nanoparticles could absorb NIR light and convert the light energy into environmental heat. The equation can be solved analytically in the steady-state regime, yielding a maximum temperature located at the surface of the nanoparticle:[6]

$$\Delta T\left(D_{\mathrm{p}}\right)=\frac{V_{\mathrm{p}}P_{\mathrm{abs}}}{2\pi k_0 D_{\mathrm{p}}} \tag{3}$$

where D_p and V_p are the diameter and volume of the nanoparticles, k_0 is the thermal conductivity of the surrounding liquid, and P_{abs} is the local light induced heating of the nanoparticle. The release of IBU is thus due to the absorption of NIR radiation by the Au-SiO_2 platforms, accelerating the release of the IBU hosted on the nanoparticle pores.

In order to confirm the feasibility of the nanoparticles in chemo-thermal therapy, we tested the cell proliferation property of the Au-SiO_2/IBU-PLL nanoparticles under NIR light irradiation as a potential material for biomedical applications. Prior to the property evaluation, the Au-SiO_2/IBU-PLL nanoparticles transfection into HeLa cell was performed with plasmid DNA (pDNA). The transfection efficiencies of the Au-SiO_2/IBU-PLL@pDNA complexes in the HeLa cell lines were higher than that of naked DNA (Figure 4b). Out of these, the efficiency for the Au-SiO_2/IBU-PLL was the highest, even higher than that from polyethyleneimine (PEI, Sigma-Aldrich, US). The percentages of green fluorescent protein (GFP) expressing cells for naked DNA, PEI, chitosan, and Au-SiO_2/IBU-PLL cases are approximately 3.3%, 48.3%, 7.6%, and 75.8%, respectively (Figure 4c). Yields were determined by the area fraction of GFP expressing cells-to-all cells in the optical microscope (with fluorescence) images. Figure 4c also shows the fluorescence of HeLa cells for the Au-SiO_2/IBU-PLL derived from the GFP expression, which further confirmed the transfection. The enhanced efficiency of the Au-SiO_2/IBU-PLL could be related to the smaller sizes than those of PEI and chitosan (*cf.* ~120 nm for PEI and ~165 nm for chitosan from the aero-fabrication with same concentrations with PLL).[22] Finally, the results (Figure 4d) show that the average cell viability only reached 26% for the Au-SiO_2/IBU-PLL particles in the presence of NIR irradiation (inset of Figure 4d) with an incubation time of 48 h, while the measured average viabilities of pure Au-SiO_2 and Au-SiO_2/IBU-PLL particles in the absence of the irradiation reached ~94% and > ~73%, respectively. The higher cytotoxicities for the Au-SiO_2/IBU-PLL without the NIR irradiation might have originated from PLL modification on the Au-SiO_2 particles (Since the cytotoxicity of PLL-modified SiO_2 nanoparticles owing to the cationic charge from the primary amine surface groups has been reported in a previous report.[23] One of the methods to minimize this is through a careful selection of the molecular weight of PLL and the complex particle concentration.) as well as Brownian diffusional release of IBU. It is observed that the Au-SiO_2/IBU-PLL particles in the presence of the irradiation exhibited efficient inhibition of cell proliferation during 48 h incubation, and there were significant differences between with and without NIR irradiation due to the chemo-thermal therapy to the HeLa cells. In addition, the pure hybrid nanoparticles verifies that they have a biocompatibility, which implies that the aero-self-assembled Au-SiO_2 nanoparticles warrant further investigation.

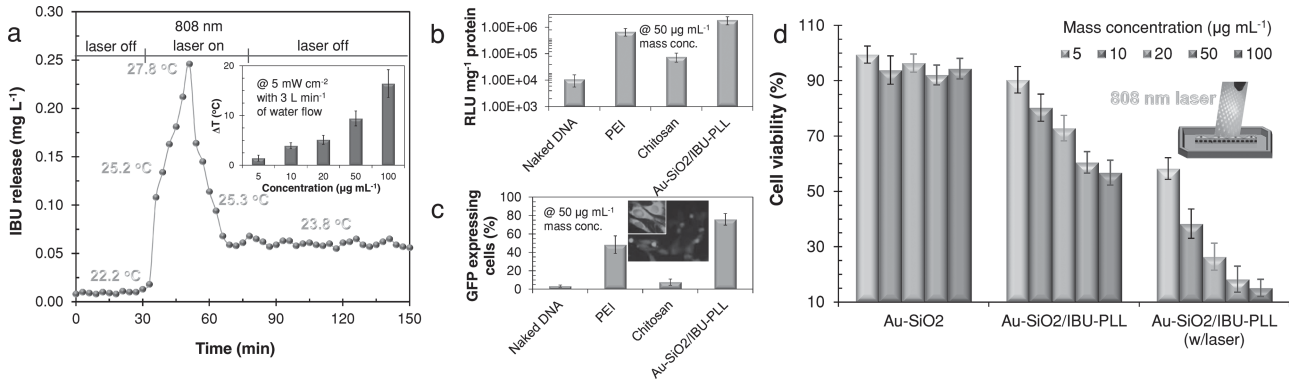

Figure 4. Results of chemo-thermal behavior of Au-SiO_2/IBU-PLL nanoparticles. (a) NIR-induced release of IBU from Au-SiO_2/IBU-PLL nanoparticles. The inset shows the temperature increases with different particle concentrations in the range of 5–100 μg mL^{-1} at 5 mW cm^{-2} light intensity with 3 L min^{-1} water flow rate. (b, c) *In vitro* measurements of the nanoparticle transfection efficiency (top: RLU mg^{-1}, bottom: GFP expressing cell %) with control particles. Low- and high-magnification fluorescent microscope images further confirm the nanoparticles transfection into HeLa cells. (d) *In vitro* measurements of cell viability versus mass concentration for the nanoparticles with and without laser irradiations.

The work presented here demonstrates that through gas-phase-based self-assembly, the Au-SiO_2 hybrid nanoparticles can be made biocompatible and suitable for linking efficient inhibition of cell proliferation through chemo-thermal therapy without any wet chemical preparations. This functional nanoparticles design approach provides useful insights for improving the applicability of Au-based hybrid nanoparticles for the development of smart controlled release systems.

Supporting Information

Supporting Information is available from the Wiley Online Library or from the author.

[1] F.-Y. Cheng, C.-T. Chen, C.-S. Yeh, *Nanotechnology* **2009**, *20*, 425104.
[2] C. Wang, C. Xu, H. Zeng, S. Sun, *Adv. Mater.* **2009**, *21*, 3045.
[3] Y. Zhai, L. Jin, P. Wang, S. Dong, *Chem. Commun.* **2011**, *47*, 8268.
[4] H. Liu, T. Liu, X. Wu, L. Li, L. Tan, D. Chen, F. Tang, *Adv. Mater.* **2012**, *24*, 755.
[5] P. Zijlstra, M. Orrit, *Rep. Prog. Phys.* **2011**, *74*, 106401.
[6] O. Neumann, A. S. Urban, J. Day, S. Lal, P. Nordlander, N. J. Halas, *ACS Nano* **2013**, *7*, 42.
[7] D. Pissuwan, S. M. Valenzueka, M. B. Cortie, *Trends Biotechnol.* **2006**, *24*, 62.
[8] R. Zanella, A. Sandoval, P. Santiago, V. A. Basiuk, J. M. Saniger, *J. Phys. Chem. B* **2006**, *110*, 8559.
[9] R. Zanella, L. Delannoy, C. Louis, *Appl. Catal. A* **2005**, *291*, 62.
[10] X. Tan, Z. Zhang, Z. Xiao, Q. Xu, C. Liang, X. Wang, *Catal. Lett.* **2012**, *142*, 788.
[11] H. Bao, B. Butz, Z. Zhou, E. Spieker, M. Hartmann, R. N. K. Taylor, *Langmuir* **2012**, *28*, 8971.
[12] C. Boissiere, D. Grosso, A. Chaumonnot, L. Nicole, C. Sanchez, *Adv. Mater.* **2011**, *23*, 599.
[13] J. H. Byeon, J. H. Park, J. Hwang, *J. Aerosol Sci.* **2008**, *39*, 888.
[14] R. Veneziano, G. Derrien, S. Tan, A. Brisson, J.-M. Devoisselle, J. Chopineau, C. Charnay, *Small* **2012**, *8*, 3674-3682.
[15] J. H. Byeon, J. T. Roberts, *ACS Appl. Mater. Interfaces* **2012**, *4*, 2693.
[16] P. K. Jain, M. A. El-Sayed, *Nano Lett.* **2007**, *7*, 2854.
[17] K. Qian, L. Luo, C. Chen, S. Yang, W. Huang, *ChemCatChem* **2011**, *3*, 161.
[18] A. C. S. Sekhar, K. Sivaranjani, C. S. Gopinath, C. P. Vinod, *Catal. Today* **2012**, *198*, 92.
[19] R. Xing, H. Lin, P. Jiang, F. Qu, *Colloid Surf. A-Physicochem. Eng. Asp.* **2012**, *403*, 7.
[20] J.-B. Kim, T. Premkumar, O. Giani, J.-J. Robin, F. Schue, K. E. Geckeler, *Macromol. Rapid Commun.* **2007**, *28*, 767.
[21] Z. Liu, X. Ma, C. Yang, F. Xu, *Vacuum* **2013**, *89*, 109.
[22] J. H. Byeon, J. T. Roberts, *Chem. Mater.* **2012**, *24*, 3544–3549.
[23] S. B. Hartono, W. Gu, F. Kleitz, J. Liu, L. He, A. P. J. Middelberg, C. Yu, G. Q. Lu, S. Z. Qiao, *ACS Nano* **2012**, *6*, 2104–2117.

Received: December 5, 2013
Revised: December 31, 2013
Published online: March 7, 2014